A high-performance, temperature-stable $Mg_{1.99}Ga_{0.01}Si_{0.99}Al_{0.01}O_4$-$CaTiO_3$ microwave dielectric ceramic and its 5G/6G waveguide filter

Huan Liu [a,&], Yu Liu [a,&], Xueqing Yu [a], Minmin Mao [a,*], Bing Liu [a], Hadi Barzegar Bafrooei [a], Aihua Li[b], Yuanyuan Zhang [b], Ehsan Taheri-Nassaj [c], Kaixin Song [a,*], Wenjun Li [a], Ian. M. Reaney [d,*]

[a] *College of Electronics Information, Hangzhou Dianzi University, Hangzhou 310018, China*

[&] *These authors contributed equally to this work and should be considered co-first authors.*

[b] *Jiaxing Glead Electronics Co., LTD, Jiaxing, Zhejiang, 314003, China*

[c] *Department of Materials Engineering, Faculty of Engineering, Tarbiat Modares University, Tehran, 14115-143, Iran*

[d] *Department of Materials, University of Sheffield, Sheffiled, S3 DJ, UK*

Abstract: New ultra-low loss, temperature-stable composite ceramics, (1-x) $Mg_{1.99}Ga_{0.01}Si_{0.99}Al_{0.01}O_4$-$x$$CaTiO_3$, have been developed with a view to expanding the portfolio of low-cost, MW dielectrics available for 5G/6G telecommunications, currently dominated by 95wt%$MgTiO_3$-5wt%$CaTiO_3$, (Mg,Ca)TiO_3 (relative permittivity, ε_r ~ 21, quality factor, $Q\times f$ ~ 56,000GHz and temperature coefficient of resonant frequency, τ_f ~ 0ppm/^{o}C). Compared with (Mg,Ca)TiO_3, 89wt%$Mg_{1.99}Ga_{0.01}Si_{0.99}Al_{0.01}O_4$-11wt%$CaTiO_3$ ceramics are also temperature stable (τ_f = -2.72 ppm/^{o}C) but have lower ε_r (~8.55) and a higher $Q\times f$ (~ 72,900GHz@12GHz and 80,900GHz@26GHz), better suited to the higher frequencies earmarked for 6G millimeter-wave (mm-wave) applications. To demonstrate its potential for 5G/6G telecommunications, a waveguide filter with novel negative coupling structure was fabricated based on simulated results. The filter had low insertion loss (0.43dB) at the center frequency (4.8GHz) and high selectivity with a roll-off rate of 576/375 dB/GHz. The S-parameters matched well at 25^{o}C and 85^{o}C, demonstrating that the filter had excellent temperature stability and was therefore suitable for future 5G/6G microwave and mm-wave communication devices.

Keywords: Microwave dielectric ceramic; Mg_2SiO_4; Filter; 5G/ 6G

1. Introduction

The next generation of wireless communication technology is developing towards fast, high efficiency and high reliability 5G/6G systems [1-3]. For 5G/6G technology, devices with low latency, low loss, and temperature stability are required. Microwave dielectric ceramics with medium permittivity ($20 \leq \varepsilon_r \leq 40$) are widely used in Beidou/GPS navigation and 4G/5G communication system such as antennas, filters, and duplexers [4, 5]. For 6G millimeter-wave (mm-wave) communication, lower ε_r is required to shorten the signal delay time (<0.1 ms) and a high-quality factor ($Q \times f$) is needed to reduce transmission loss. Any device must also have near-zero temperature coefficient of resonant frequency (τ_f) to be stable under different working ambient conditions [6-10].

Bandpass filters have been reported for applications at 5G-Sub 6GHz frequencies, based on $Ca_2YZr_{1.7}Ti_{0.3}Al_3O_{12}$, $Ba(Mg_{1/3}Ta_{0.675})O_3$, $LiMg_{0.9}Zn_{0.06}Ni_{0.04}TiO_2$ and $AgMgVO_4$ ceramics[11-14]. Microstrip patch and dielectric resonator antennas have also been reported for GPS/Beidou navigation, 5G/6G-sub 6GHz and mm-wave frequency band using $Y_{2.95}Dy_{0.05}MgAl_3SiO_{12}$, $Sr_{3-x}Ca_xV_2O_8$, $Li_2Ti_{0.8}(Cu_{1/3}Nb_{2/3})_{0.2}O_3$ and $Y_3Al_5O_{12}$ as ceramic substrates [15-18]. Though the above microwave ceramics have a high $Q \times f$ and near zero τ_f, greater synergy is required between permittivity, high-quality factor and temperature stability.

Forsterite (Mg_2SiO_4) is an important silicate for the 6G mm-wave band owing to its low ε_r = 6.8, ultra-high $Q \times f$ =240,000 GHz and adjustable τ_f [19-21]. However, the –ve τ_f (-70ppm/^{o}C) of Mg_2SiO_4 and the appearance of secondary phase such as $MgSiO_3$ decrease its $Q \times f$. Song et al. designed the strategy of Mg/Si non-stoichiometric ratio (Mg/Si = 2.05) to suppress the secondary phase of $MgSiO_3$ for single-phase Mg_2SiO_4 with ε_r ~ 7.5, $Q \times f$ ~ 114,730 GHz@10.57 GHz and τ_f ~ -59 ppm/^{o}C [22]. Yue et al. adjusted the τ_f of Mg_2SiO_4 to 0.6ppm/°C by the addition of 45%$Ba_3(VO_4)_2$ and obtained ε_r ~ 9.03 and $Q \times f$ ~ 52,500 GHz@11.3GHz [23]. Feng et al. obtained composite ceramics 94 wt%Mg_2SiO_4 (Mg/Si = 2.05)-6 wt%$Ca_{0.9}Sr_{0.1}TiO_3$ with excellent microwave dielectric properties (ε_r ~ 8.01, $Q \times f$ ~ 58,389 GHz@14.6 GHz and τ_f ~-3.62 ppm/^{o}C) [24]. Dou et al. used $CaTiO_3$ to adjust its τ_f and used

Bi_2O_3-Li_2CO_3-B_2O_3 as glass sintering additives to realize the low temperature co-sintering 91wt%Mg_2SiO_4-9wt%$CaTiO_3$ ceramics @ 950°C with ε_r ~ 7.7, $Q\times f$ ~ 11,300 GHz@6.1 GHz and τ_f ~ -5ppm/°C [25]. Tong et al. prepared Mg_2SiO_4 by Mg/Si non-stoichiometric ratio, and then prepared the low temperature co-sintering 90wt%Mg_2SiO_4-10wt%$CaTiO_3$ @ 900°C using 2wt%ZBS-1.5wt%LiF as sintering additives with ε_r ~ 9.26, $Q\times f$ ~ 68,580GHz@15.5GHz and τ_f ~ -1.49ppm/°C [26]. The present authors further succeeded to reduce the volume fraction of secondary $MgSiO_3$ phase using Ga^{3+} and Al^{3+} for Mg^{2+} for Si^{4+} respectively, rather than Mg/Si non-stoichiometric ratio, to produce $Mg_{0.99}Ga_{0.01}Si_{0.99}Al_{0.01}O_4$ with charge balance which sintered at 1450 °C and gave ε_r = 6.96, $Q\times f$ = 230, 000GHz@12.6GHz and τ_f = -38ppm/°C.

In this study, the large –ve τ_f (-38ppm/°C) in $Mg_{0.99}Ga_{0.01}Si_{0.99}Al_{0.01}O_4$ is compensated by the +ve τ_f of $CaTiO_3$ [22] to produce composites based on (1-x) $Mg_{0.99}Ga_{0.01}Si_{0.99}Al_{0.01}O_4$-$x$$CaTiO_3$. The effect of $CaTiO_3$ content on microstructure, vibrational modes and mm-wave dielectric properties was investigated and a dielectric waveguide bandpass filter with new negative coupling is designed and fabricated based on the optimum composition (x = 11wt%) to demonstrate potential applications in 5G/6G communications.

2. Experimental procedure

$Mg_{1.99}Ga_{0.01}Si_{0.99}Al_{0.01}O_4$ (MGSA) ceramics were fabricated through the conventional solid-state reaction approach employing high-grade purity MgO (99.99%), Ga_2O_3 (99.99%), Al_2O_3 (99.99%), SiO_2 (99.5%) as raw materials, all of which were purchased from Aladdin Chemical Co. Ltd in China. Raw materials were weighed based on the stoichiometric formula and milled in polyethylene bottle with ZrO_2 media in ethyl alcohol for 24h. The milled slurry was dried and calcined at 1150°C for 4h. $CaTiO_3$ (99.9%) with different mass fractions was added into MGSA powder and ball milled. The re-milled powders were dried, mixed with 10wt% polyvinyl alcohol (PVA) as a binder, and then sieved (100 mesh). The powders were die pressed into 12mm diameter and 3-5mm height discs at 120MPa, then sintered in

air at 1250-1400ºC for 3h on alumina plates at a heating rate of 4ºC /min.

The crystal structure and phase composition were analyzed on powder of crushed ceramics by X-ray diffraction using Cu Kα radiation (XRD, Rigaku Smart Lab SE, Japan). The results were analyzed by the Rietveld profile refinement method with the FULLPROF program. The microstructures and the elemental distributions of the polished and thermal-etched surfaces of MGSA-$CaTiO_3$ ceramics were investigated using a scanning electron microscope (SEM, ZEISS Sigma 300, Germany) equipped with energy dispersive spectroscopy (EDS). The thermal etching process was conducted at a temperature 50 ºC lower than the sintering temperature for 30min. The average grain size was determined from the SEM micrographs by the lineal intercept method (using ImageJ software). The ceramic samples were carefully polished with diamond slurry to a roughness of about 0.5 μm for Raman test. Raman spectra were obtained using a Horiba Evo Nano spectrometer with a green excitation laser (λ = 532 nm). Microwave dielectric properties were measured using a network analyzer (N5234B, Keysight, America). The temperature coefficient of resonant frequency (τ_f) was calculated using Eq. (1):

$$\tau_f = \frac{f_H - f_L}{(T_H - T_L) \times f_L} \times 10^6 (\text{ppm/℃}) \quad (1)$$

where f_L, f_H represent the resonant frequency at T_L (25ºC) and T_H (85ºC), respectively.

3. Results and discussion

3.1. Characterization of (1-x)wt%MGSA-xwt%$CaTiO_3$ ceramics

Fig. 1(a) shows the XRD patterns of (1-*x*)MGSA-*x*$CaTiO_3$(8wt% ≤ *x* ≤ 13wt%) samples at 1350℃ for 3h. The main phase matches well with the Mg_2SiO_4 profile on standard PDF card #80-0944.The (400) and (022) diffraction peaks of $CaTiO_3$ appear at ~33° and 48° 2θ, corresponding to PDF card #82-0228. The intensity of both peaks gradually increases, as a function of *x*, with no impurity peaks present, thereby demonstrating that $CaTiO_3$ may coexist with MGSA to form a dual-phase composite with no or limited interaction. Fig. 1(b) shows a XRD diagram of 89wt%%MGSA-11wt%$CaTiO_3$ refined (Rietveld) using Fullprof software. The corresponding

refinement results were R_p = 9.31 and R_{wp} = 13.5, χ^2 = 4.6. The mass fraction of MGSA and $CaTiO_3$ were determined as 88.7wt% and 11.3wt%, respectively, similar to the batched formulation.

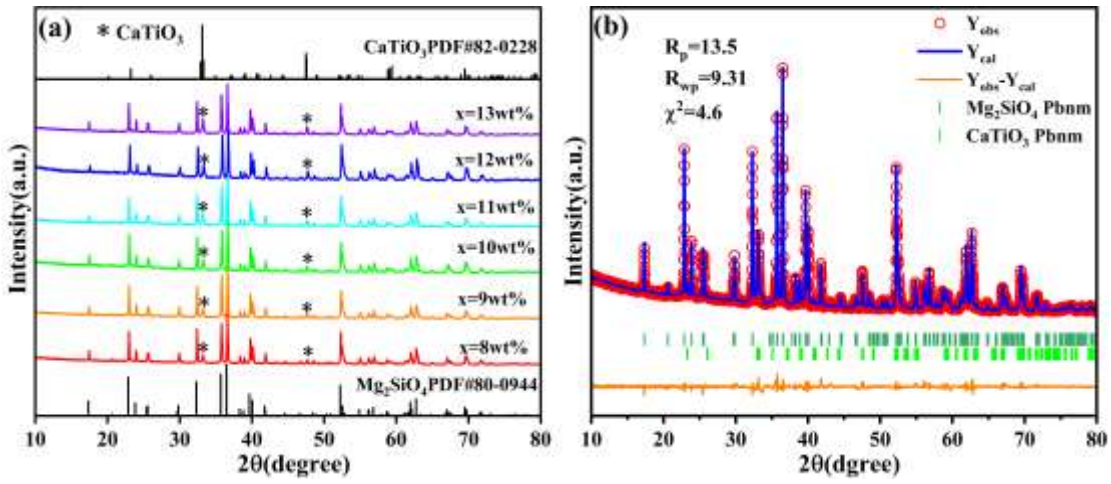

Fig. 1. (a) XRD pattern of (1-*x*)MGSA-*x*$CaTiO_3$(8wt% ≤ *x* ≤ 13wt%). (b)Rietveld refined results patterns of 89wt%MGSA-11wt%$CaTiO_3$ ceramics specimens.

Fig. 2 shows SEM micrographs of thermally etched (1-*x*)MGSA-*x*$CaTiO_3$ composite ceramics. All samples exhibit a dense microstructure and there are relatively few pores. In order to further verify the distribution of (1-x)MGSA-x$CaTiO_3$ composite ceramics, the elements composition of grains were analyzed by EDS. The EDS results are shown in S1. The distribution of MGSA and $CaTiO_3$ can be clearly distinguished with the lighter and darker contrast grains in the SEM image. As $CaTiO_3$ content (*x*) increases, the average grain size shows a trend of first increasing and then decreasing, MGSA grains increasingly appear in lath-shaped. For *x*≥11wt%, all MGSA grains are lath-like, Fig. 2(b)-2(c) which may be detrimental to *Q*×*f*.

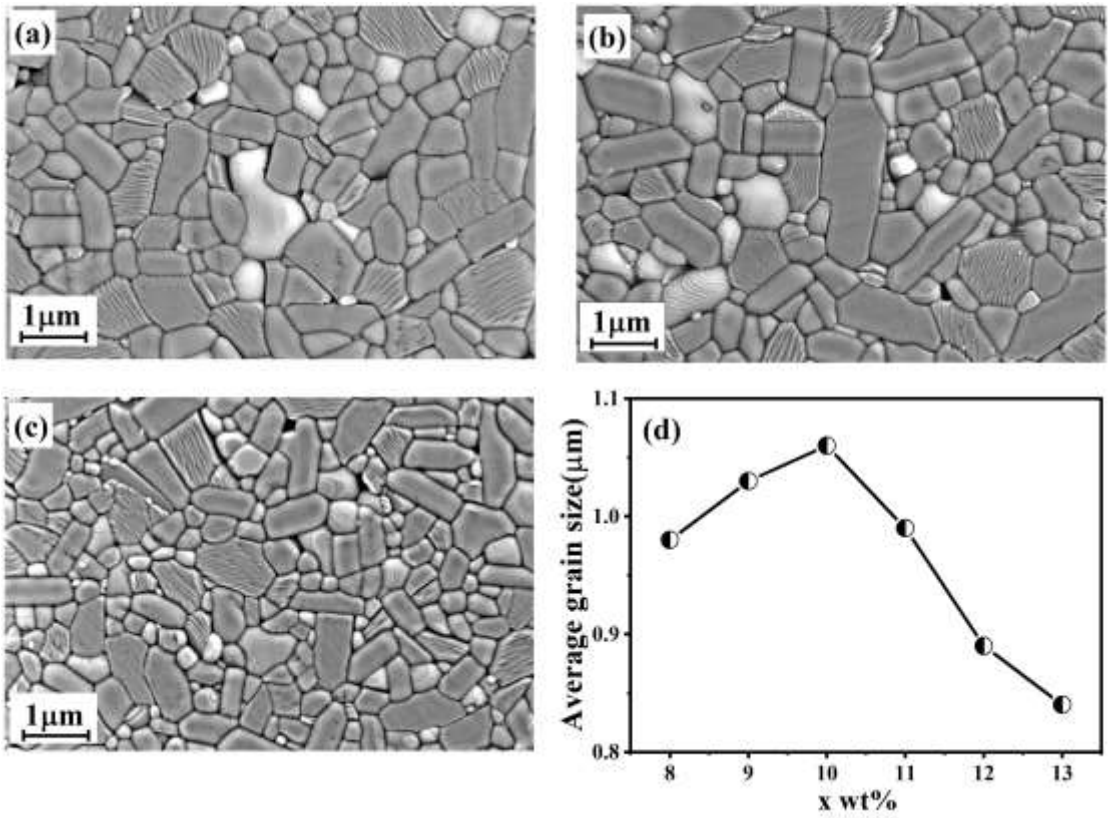

Fig. 2. The thermal etched SEM image of (1-*x*)MGSA-*x*$CaTiO_3$: (a) *x*=9wt%, (b) *x*=11wt%, (c) *x*=13wt% sintered at optimum temperature, (d) average grain size.

Fig.3 (a) shows the Raman spectra of (1-*x*)MGSA-*x*$CaTiO_3$ (8wt% ≤ *x* ≤ 11wt%) composite ceramics which illustrate the vibrational modes present in the composite ceramic [27, 28] As a comparison, Raman spectra of MGSA and $CaTiO_3$ were also obtained. Fig. 3(b) shows five characteristic peak positions of $CaTiO_3$ corresponding to 191cm^{-1}, 241cm^{-1}, 339cm^{-1}, 464cm^{-1}, 780cm^{-1}, respective1y and four characteristic peak positions of MGSA at 229cm^{-1}, 306cm^{-1}, 826cm^{-1}, 859cm^{-1}, respective1y [29]. The Raman peaks observed at 149cm^{-1} can be attributed to the stretching vibrations of the Ca-O bond and the peaks at 241cm^{-1} and 339cm^{-1} correspond to stretching vibrations and bending vibrations of the [TiO_6] tetrahedra. The Raman peaks observed at 186cm^{-1} and 306cm^{-1} are attributed to stretching vibrations of the Mg-O bond, while the peak at 464cm^{-1} is assigned to bending vibrations of the Ti-O bond. Additionally, the peak appearing at 780cm^{-1} is associated with the symmetric tensile vibration of the [TiO_6] octahedra and those at 826cm^{-1} and 859cm^{-1} are stretching vibrations of the Si-O bond. With increasing *x*, the intensity of the characteristic

MGSA peaks decreased and the Raman peak of 859cm^{-1} shifted to the left. The Raman spectra indicate that MGSA coexists with limited or no interaction with $CaTiO_3$ in the composite ceramic, consistent with XRD and SEM results.

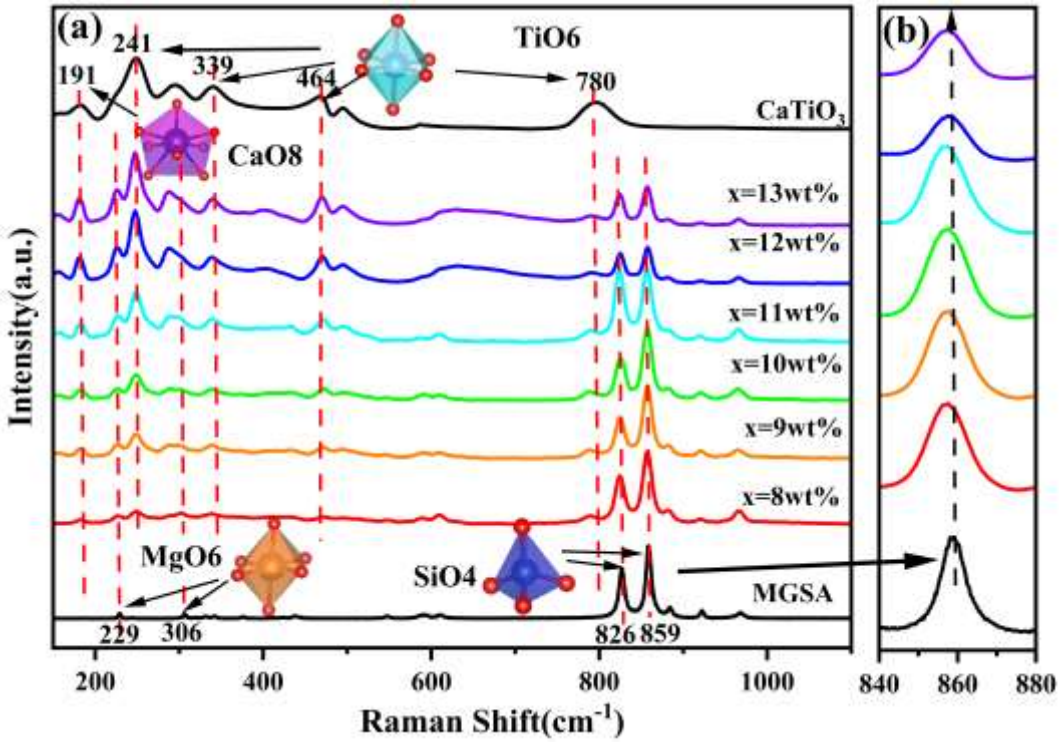

Fig. 3. (a) Raman spectrum of (1-*x*)MGSA-*x*$CaTiO_3$ composite ceramics. (b) Enlarged Raman spectrum between 840-880cm^{-1}.

3.2. Microwave dielectric properties of ceramics

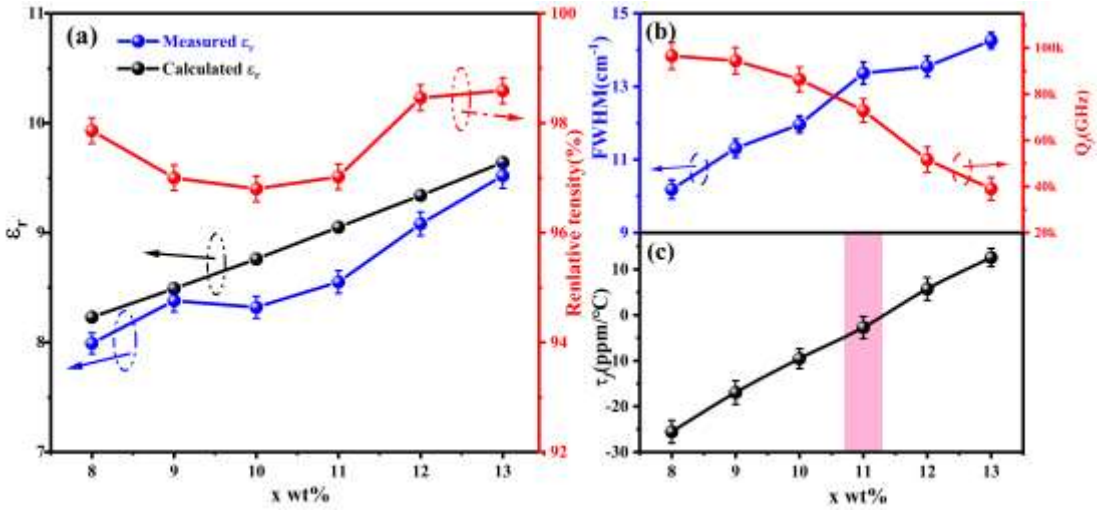

Fig. 4. (a) The variation of ε_r and relative density. (b) FWHM of the peaks at 859 cm^{-1}and $Q\times f$ at 12GHz of (1-*x*)MGSA-*x*$CaTiO_3$ as a function of composition *x* value. (c) The τ_f of (1-*x*)MGSA-*x*$CaTiO_3$ as a function of composition *x* value.

Fig. 4(a) illustrates the relative density along with the measured and calculated ε_r with respect to composition. For all compositions, measured ε_r increases with x with only a slight deviation from this trend for x = 8wt%, presumably due to increased porosity. All measured ε_r values are lower than theoretical owing to the existence of pores in the ceramic. Fig. 4(b) shows the full width at half maximum (FWHM) of the Raman peaks at 859cm^{-1} and $Q\times f$ at 12GHz as a function of composition. $Q\times f$ decreases as x increases but the FWHM increases. The trends of FWHM for Raman peaks and $Q\times f$ values are opposed because of enhancement in damping of the stretching mode as the FWHM increases, leading to higher intrinsic losses. The relation between $tan\delta$ and FWHM is associated with the damping coefficient (γ), according to Eqs. (2) and (3) [30].

$$\tan\delta = \frac{\gamma\omega_0}{\omega_T^2} \tag{2}$$

$$\text{FWHM} = \frac{\gamma\sqrt{\gamma^2 + 4\omega_0^2}}{2\omega_0} \tag{3}$$

where γ, ω_0, and ω_T represent damping coefficient, central frequency of optical mode, and angular frequency of lattice vibration, respectively. Fig. 4(c) shows the variation in τ_f for (1-x) MGSA-xCaTiO$_3$ ceramics sintered at the optimum temperature. τ_f gradually increases to a positive value with increasing x, with x = 11wt% close to zero (τ_f ~ -2.72 ppm/^{o}C) with ε_r ~ 8.55 and $Q\times f$ ~ 72,900GHz@12GHz; properties suitable for 5G/6G applications.

To assess the suitability of 6G communications (mm-wave), $Q\times f$ was measured using the TE$_{011}$ mode at 26GHz (Fig. 5) with the dimensions adjusted accordingly. At 26GHz, $Q\times f$ was 80,900GHz, higher than at 12GHz (72,900GHz), possibly due to the smaller test piece having statistically fewer defects [31], thereby confirming their potential for mm-wave applications. Table 1 compared the data of proposed 89wt%MGSA-11wt%CaTiO$_3$ ceramics with the previously reported forsterite relevant ceramics. The strategy of Mg^{2+}-Ga^{3+} synergistic substitution of Si^{4+}-Al^{3+} in Mg_2SiO_4 by stoichiometric ratio and charge balance, that effectively inhibited the formation of the second phase MgSiO$_3$. Moreover, the prepared 89wt%MGSA-11wt%CaTiO$_3$

ceramics shows excellent $Q\times f$ and near-zero τ_f in microwave and mm-wave band, which indicates that the ceramics have broader application prospects in current 5G telecommunications and the future next generation mm-wave communication.

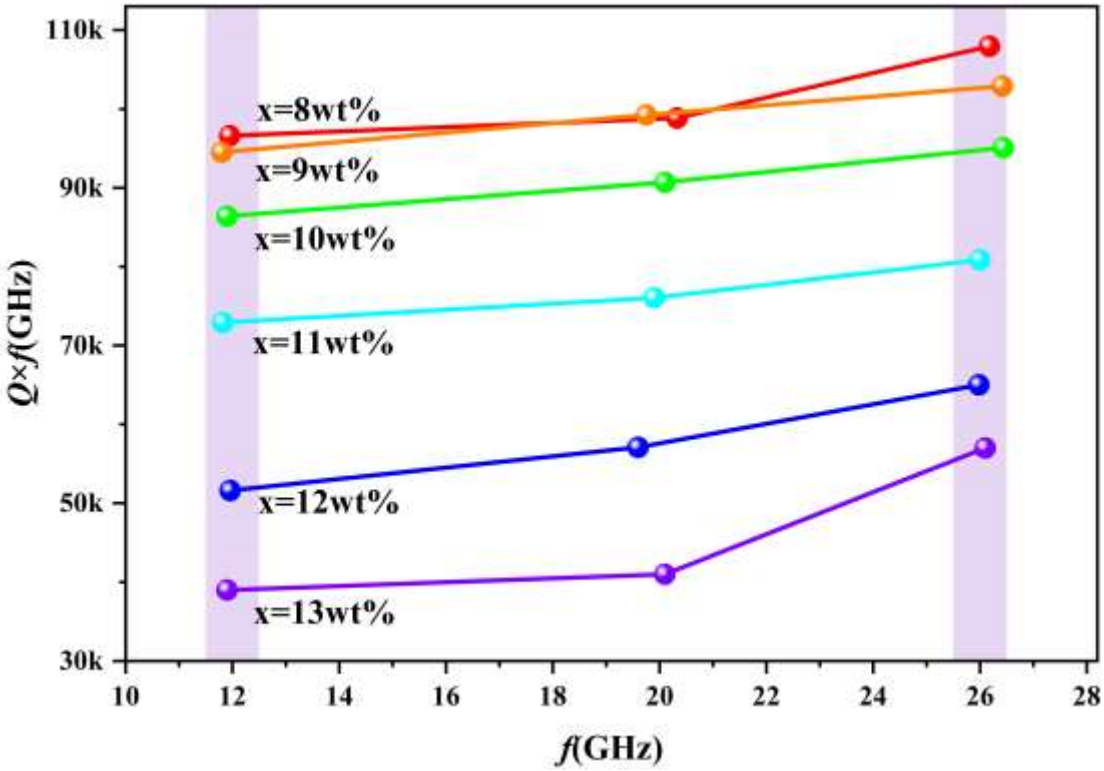

Fig. 5. Variation of $Q\times f$ value as a function of frequency for selected (1-x)MGSA-$x$$CaTiO_3$.

Table 1

Some of the reported adjust τ_f of Mg_2SiO_4

Ceramics composition	ε_r	$Q\times f$(GHz)	τ_f (ppm/°C)
Mg_2SiO_4(non-stoichiometric ratio of Mg/Si = 2.05)	7.5	114,730@10.57GHz	-3[22]
55wt%Mg_2SiO_4-45wt%$Ba_3(VO_4)_2$	9.03	52,500@11.3GHz	0.6[23]
94wt%Mg_2SiO_4-6wt%$Ca_{0.9}Sr_{0.1}TiO_3$	8.01	58,389@14.6GHz	-3.62[24]
91wt%Mg_2SiO_4-9wt%$CaTiO_3$-12wt%BLB	7.7	11,300@6.1GHz	-5[25]
90wt%Mg_2SiO_4-10wt%$CaTiO_3$-2wt%ZBS-1.5wt%LiF	9.26	68,580@15.5GHz	-1.49[26]
89wt%$Mg_{1.99}Ga_{0.01}Si_{0.99}Al_{0.01}O_4$-11wt%$CaTiO_3$	8.55	72,900@12GHz	-2.72[this work]
89wt%$Mg_{1.99}Ga_{0.01}Si_{0.99}Al_{0.01}O_4$-11wt%$CaTiO_3$	8.55	80,900@26GHz	-2.72[this work]

*: Accurate data is not provided in the literature, and it is estimated data.

3.3. Design of low-loss dielectric waveguide bandpass filter based on 89wt%MGSA-11wt%$CaTiO_3$ ceramics

With the application of massive antenna arrays technology in 5G communication, the number of filters has increased sharply, leading to a requirement for smaller and lightweight filters. Dielectric waveguide filters offer unique advantages such as low loss, compact shape, and light weight. Therefore, the application of 89wt%MGSA-11wt%$CaTiO_3$ as dielectric waveguide bandpass filter was investigated. The filter (Fig. 6 (a) and 6 (b)) is composed of four resonant units, three positive coupling windows, two negative coupling holes, and two ports. The negative coupling adopts a new structure of symmetrical shallow blind holes, unlike traditional single deep blind hole, which helps to achieve more uniform metallization of blind holes and improve the manufacturing accuracy of filters. According to the theory of rectangular waveguide resonators and the coupling design methods [32-35], the design details of the filter are shown in the Supplementary Information, and the optimal physical size (22.4mm×22.4mm×6.2mm) of the proposed filter is shown in Table 2. The proposed filter's electric field intensity distribution was calculated at 4.8GHz in Fig. 6(c), which proves the coupling mechanism of the designed structure. The proposed filter was manufactured (Fig. 6(d)), and the measured S-parameter curve was consistent with the simulation, as shown in Fig. 6(e). The measured insertion loss was 0.43dB at center frequency and the steep roll-off rate were 576/375 dB/GHz. Compared with the other reported dielectric waveguide filters, the proposed filter had lower insertion loss and high frequency selectivity [33, 36]. Additionally, the response of the filter at 25^{o}C and 85^{o}C was measured in the high and low temperature test chamber, and the S-parameters remain constant at different temperatures, as shown in Fig. 6(f)-(h). These results imply that 89wt%MGSA-11wt%$CaTiO_3$ ceramics have potential application in mobile communication systems.

Table 2

The key physical dimensions of the dielectric waveguide filter.

Parameters	h_1	h_2	h_{23}	h_p	d	d_1	d_2	w_{12}	l_{12}	w_{14}	l_{14}
Values (mm)	2.71	2.94	2.67	1.39	1.7	1.8	0.75	2.73	0.895	2.89	3.505

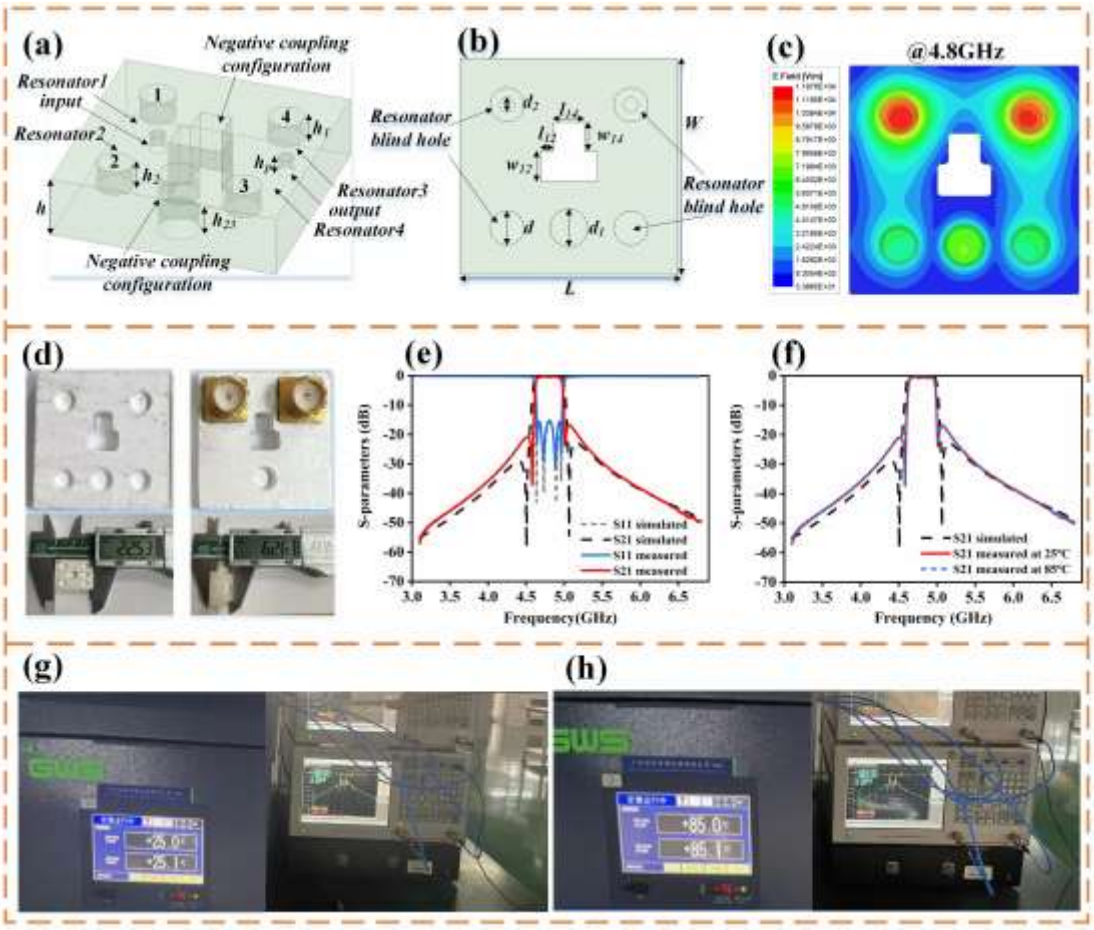

Fig. 6. Configuration and results of the proposed filter: (a) perspective view, (b) top view, (c) the electric field distribution at 4.8 GHz, (d) the fabricated photograph, (e) simulated and measured insertion loss (S_{21}) and return loss (S_{11}) at room temperature, (f) simulated and measured S_{21} at 25ºC and 85ºC, and (g),(h) measured S-parameter at 25ºC and 85ºC, respectively.

4. Conclusion

(1-x)$Mg_{1.99}Ga_{0.01}Si_{0.99}Al_{0.01}O_4$-$x$$CaTiO_3$ composite ceramics were prepared by solid-state reaction and their structure, microstructure and phase assemblage were investigated using X-ray diffraction, Raman spectroscopy, SEM and EDS. No reaction was detected between the two end members and 89wt%MGSA-11wt%$CaTiO_3$ ceramics exhibited superb microwave dielectric properties (ε_r ~8.55, higher $Q\times f$ ~ 80,900GHz@26GHz and τ_f ~ -2.72 ppm/ºC). A novel dielectric waveguide bandpass filter with new negative structure was fabricated from x = 11wt% and its performance

determined at 25°C and 85°C with each S-parameters almost identical. The filter therefore was temperature stabile, had low insertion loss of 0.43dB at 4.8GHz, and high selectivity with a roll-off of 576/375 dB/GHz, suitable for 5G/6G communications.

Declaration of Competing Interest

The authors declare that they have no known competing financial interests or personal relationships that could have appeared to influence the work reported in this paper.

Acknowledgments

This work was supported by the National Natural Science Foundation of China (Grant no. 52161145401 and 51672063).

References

[1] N. Joseph, J. Varghese, M. Teirikangas, T. Vahera , H. Jantunen, Ultra low temperature cofired ceramic substrates with low residual carbon for the next generation microwave applications, ACS Appl. Mater. Interfaces 11 (26) (2019) 23798–23807.

[2] Y. Xiong, Z. Xing, J.H. Weng, C. Ma, J. Khaliq, C.C. Li, Low-temperature sintering, dielectric performance, and far-IR reflectivity spectrum of a lightweight $NaCaVO_4$ with good chemical compatibility with silver, Ceram. Int. 47 (15) (2021) 22219–22224.

[3] F. Li, Y. Li, J. Zhang, X. Liu, Y. Lu, R. Peng, Y. Liao, T. Tang, X. Wu, Q. Wen. 5G array antenna substrate for electromagnetic beam splitting via cobalt-substituted zinc molybdate low temperature co-fired ceramics, J. Eur. Ceram. Soc. 42 (13) (2022) 5771–5777.

[4] I.M. Reaney, D. Iddles, Microwave dielectric ceramics for resonators and filters in mobile phone networks, J. Am. Ceram. Soc. 89 (7) (2006) 2063–2072.

[5] H.C. Xiang, J. Kilpijärvi, S. Myllymäki, H.T. Yang, L. Fang, H. Jantunen, Spinel-

olivine microwave dielectric ceramics with low sintering temperature and high quality factor for 5GHz wi-fi antennas, Appl. Mater. Today 21 (2020) 100826.

[6] Y. Jiang, H. Liu, Z.Y. Xiu, G.F. Wu, M.M. Mao, X.J. Luo, B. Liu, Z.L. Lu, Z.M. Qi, D.Y. Sun, K.X. Song, Temperature-stable $Y_{2.95}Dy_{0.05}MgAl_3SiO_{12}$ garnet-type 5G millimeter-wave dielectric ceramic resonator antenna, Ceram. Int. 48 (23) (2022) 35085–35091.

[7] S. Li, C. Li, M.M. Mao, K.X. Song, Y. Iqbal, A. Khesro, S. Faouri, Z.L. Lu, B. Liu, S.K. Sun, D.W. Wang, High $Q\times f$ values of Zn-Ni co-modified $LiMg_{0.9}Zn_{0.1-x}Ni_xPO_4$ microwave dielectric ceramics for 5G/6G LTCC modules, J. Eur. Ceram. Soc. 42 (13) (2022) 5684–5690.

[8] Z. Fang, L.X. Pang, D. Zhou, X.L. Wang, S. Ren, W.G. Liu, Phase compositions and microwave dielectric characteristics of $x$$Mg_2B_2O_5$-(1-$x$)$Ba_3V_2O_8$($0.5\leq x\leq 0.7$) ceramics, J. Alloy. Compd. 933 (2023) 167662.

[9] L. He, R. Zuo, A novel (1-x) $MgZr_{0.85}Sn_{0.15}Nb_2O_{8-x}$$Ba_3Ti_4Nb_4O_{21}$ microwave dielectric composite ceramic with near-zero temperature coefficient, J. Alloy. Compd. 896 (2022) 163101.

[10] Y. Gao, J. Jiang, J. Wang, L. Gan, X.M. Jiang, T.J. Zhang, $Li_{2+x}ZrO_3F_x$ ($0\leq x\leq 1.25$): A new high $Q\times f$ and temperature-stable microwave dielectric ceramic system for LTCC applications, J. Am. Ceram. Soc. 106 (3) (2023) 1881–1891.

[11] X.Q. Song, F. F. Zeng, J. Q. Yang, C. Z. Yin, J. M. Wu, Y. S. Shi, W. Z. Lu, W. Lei, Crystal structure and microwave dielectric properties of garnet-type $Ca_2YZr_{2-x}Ti_xAl_3O_{12}$ ceramics for dual-band bandpass filters, J. Eur. Ceram. Soc. 42 (12) (2022) 4962–4968.

[12] M.K. Du, L.X. Li, L.Z. Ni, Y. Zhan. Ultra-high Q $Ba(Mg_{1/3}Ta_{0.675})O_3$ microwave dielectric ceramics realized by slowly cooling step process and the simulation design for hairpin dielectric filters, Ceram. Int. 47 (14) (2021) 19716–19726.

[13] L. Chen, H. Liu, Y. Jiang, S. Li, X.J. Luo, B. You, A.H. Li, Y.Y. Hu, H. Baxter, B. Yang, M.M. Mao, H.B. Bafrooei, W.J. Li, K.X. Song, High quality of $LiMg_{0.9}Zn_{0.06}Ni_{0.04}PO_4$-$TiO_2$ microwave ceramic and its application for 5G dielectric waveguide bandpass filter, Mater. Today Commun. 35 (2023) 105500.

[14] C.-L. Huang, T.-H. Hsu, Ultra-low temperature sintering and temperature stable microwave dielectrics of phase pure $AgMgVO_4$ ceramics, J. Eur. Ceram. Soc. 42 (9) (2022) 3892–3897.

[15] Y. Jiang, H. Liu, Z. Xiu, G. Wu, M. Mao, X. Luo, B. Liu, Z. Lu, Z. Qi, D. Sun, K. Song, Temperature-stable $Y_{2.95}Dy_{0.05}MgAl_3SiO_{12}$ garnet-type 5G millimeter-wave dielectric ceramic resonator antenna, Ceram. Int. 48 (23) (2022) 35085–35091.

[16] C.Z. Yin, Y.H. Yin, K. Du, X.Q. Song, H.H. Guo, Y. Xiong, M.F. Cheng, J.Q. Yang, W. Luo, W.Z. Lu, W. Lei, C.C. Li, Fabrication of high-efficiency dielectric patch antennas from temperature-stable $Sr_{3-x}Ca_xV_2O_8$ microwave dielectric ceramic, J. Eur. Ceram. Soc. 43 (4) (2023) 1492–1499.

[17] H.H. Guo, M.S. Fu, D. Zhou, C. Du, P.J. Wang, L.X. Pang, W.F. Liu, A.S.B. Sorbra, J.Z. Su. Design of a High-Efficiency and -Gain Antenna Using Novel Low-Loss, Temperature-Stable $Li_2Ti_{1-x}(Cu_{1/3}Nb_{2/3})_xO_3$ Microwave Dielectric Ceramics, ACS Appl. Mater. Interfaces. 13 (1) (2021) 912–923.

[18] C. Du, M. Fu, D. Zhou, H. Guo, H. Chen, J. Zhang, J. Wang, S. Wang, H. Liu, W. Liu, L. Li, Z. Xu, Dielectric resonator antenna with $Y_3Al_5O_{12}$ transparent dielectric ceramics for 5G millimeter-wave applications, J. Am. Ceram. Soc. 104 (9) (2021) 4659–4668.

[19] T. Tsunooka, M. Androu, Y. Higashida, H. Ohsato, Effects of TiO_2 on sinterability and dielectric properties of high-Q forsterite ceramics, J. Eur. Ceram. Soc. 23 (14) (2003) 2573–2578.

[20] H. Ohasto, T. Tsunooka, M. Ando, Y. Ohishi, Y. Miyauchi, K. ichi Kakimoto, Millimeter-wave Dielectric Ceramics of Alumina and Forsterite with High Quality factor and Low Dielectric Constant, J. Korean Ceram. Soc. 40 (4) (2003) 350-353.

[21] H. Ohsato, T. Tsunooka, A. Kan, Y. Ohishi, Y. Miyauchi, Y. Tohdo, T. Okawa, K. Kakimoto, H. Ogawa, Microwave-millimeterwave dielectric materials, Key Eng. Mater. 269 (2004) 195–198.

[22] K.X. Song, X.M. Chen, X.C. Fan, Effects of Mg/Si Ratio on Microwave dielectric characteristics of forsterite ceramics, J. Am. Ceram. Soc. 90 (2007) 1808–1811.

[23] S. Meng, Z. Yue, H. Zhuang, F. Zhao, L. Li, Microwave Dielectric Properties of $Ba_3(VO_4)_2$–Mg_2SiO_4 Composite Ceramics, J. Am. Ceram. Soc. 93 (2) (2010) 359–361

[24]L. Liu, Y. Feng, T. Qiu, X. Li, Microstructures and microwave dielectric properties of Mg_2SiO_4–$Ca_{0.9}Sr_{0.1}TiO_3$ ceramics, J. Mater. Sci. Mater. Electron. 26 (2015) 1316–1321.

[25] G. Dou, D. Zhou, M. Guo, S. Gong, Y. Hu, Low-temperature sintered Mg_2SiO_4–$CaTiO_3$ ceramics with near-zero temperature coefficient of resonant frequency, J. Mater. Sci.-Mater. El. 24 (5) (2013) 1431–1438.

[26] C. Tang, Y. Xin, C.X. Zhang, J.G. Tan, Z.G. Yu, C.C. Wu, J.X. Tong, F.C. Meng, Effects of ZBS addition on crystallization, microstructure and dielectric properties of low temperature co-fired Mg_2SiO_4-$CaTiO_3$ ceramics, J Electroceram. 50 (2023) 44–49.

[27] D. Zhou, L.X. Pang, H. Wang, J. Guo, X. Yao, C.A. Randall. Phase transition, Raman spectra, infrared spectra, band gap and microwave dielectric properties of low temperature firing $(Na_{0.5x}Bi_{1-0.5x})(Mo_xV_{1-x})O_4$ solid solution ceramics with scheelite structures, J. Mater. Chem. 21 (45) (2011) 18412–18420.

[28] G. Gouadec, P. Colomban, Raman Spectroscopy of Nanomaterials: How Spectra Relate to Disorder, Particle Size and Mechanical Properties, Prog. Cryst. Growth. Ch. 53 (1) (2007) 1–56.

[29] P.K. Lam, R. Yu, M.W. Lee, S.K. Sharma, Structural Distortions and Vibrational Modes of Mg_2SiO_4, Am. Mineral. 75 (1) (1990) 109–119.

[30] F. Huang, H. Su, Q. Zhang, X.H. Wu, Y.X. Li, X.L. Tang, Na-doped diopside microwave ceramics with dielectric properties influenced by the sintering, lattice vibration and chemical bond characteristics, J. Alloys Compd. 896 (2022), 162973.

[31] L. Li, X.M. Chen, Frequency-dependent $Q\times f$ value of low-loss $Ba_2Ti_9O_{20}$ ceramics at microwave frequencies, Ceram. Int. 38 (8) (2012) 6831–6835.

[32] D.M. Pozar, Microwave Engineering. New York: Wiley 6 (2011) 285.

[33] Y. Chen, Y. Zhang, K.-L. Wu, A Dual-Mode, Monoblock dielectric bandpass filter using dissimilar fundamental modes, IEEE Trans. Microw. Theory Tech. 69 (8) (2021) 3811–3819.

[34] J.S. Hong and M.J. Lancaster, Microstrip filters for RF/Microwave Applications.

New York, NY, USA: Wiley. 9 (2001) 266.

[35] J.S. Hong and M.J. Lancaster, Microstrip filters for RF/Microwave Applications. New York, NY, USA: Wiley. 8 (2001) 215-218.

[36] W. Qin, J. Liu, W.W. Yang, J.X. Chen, Y.C. Li, R.L. Xu, Integrated-designs of filtering circuits based on adjustable dielectric waveguide resonators, IEEE Trans. Circuits Syst. II, Exp. Briefs. 69 (2) (2021) 284–288.